Mathematical Theory and Modeling
ISSN 2224-5804 (Paper) ISSN 2225-0522 (Online)
Vol.9, No.11, 2019

Evaluation of Phase Perturbations induced by the Presence of Sea-foam on the Surface of the Ocean using Padé Approximation

Collins E. Ouserigha[1*] Ayibapreye K. Benjamin[2]

1. Department of Physics, Niger Delta University, P.M.B 071 Yenagoa, Bayelsa State, Nigeria
2. Department of Electrical/Electronic Engineering, Niger Delta University, Yenagoa, Nigeria

* E-mail of the corresponding author: ouserigha.ec@ndu.edu.ng

Abstract

This paper reports phase perturbations induced by the presence of sea-foam on the surface of the ocean, when an incident electromagnetic wave (EM) at WindSat frequencies 10.7 GHz and 37 GHz was propagated through a foam-covered sea-foam layer modelled as sequences of phase scattering screens. The propagation process was modelled by Parabolic-Wave Equation (PWE) and solved by Padé approximation. The parabolic equation has been widely used to solving EM scattering and radio wave propagation problems. The split-step Pade's approximation method is used in computation of the phase perturbations that occurs within the sea-foam layer due to the presence of varying effective dielectric constant of closely packed air-bubbles in the sea-surface. Results obtained show variation of the propagated E-fields through slices of sea-foam layer as functions of foam frequency, foam layer thickness, polarization and angle of incidence.

Keywords: Phase perturbation, sea foam, Padé approximation

1. Introduction

It has been realized that parabolic equation (PE) method may be adopted as an efficient numerical tool for EM field calculation and may bridge the gap between rigorous numerical methods such as method of moments (MOM) and finite difference time domain (FDTD), and asymptotic methods based in ray tracing or physical optics. Applying PE method can avoid the limitation of central processing unit (CPU) time and memory required by these rigorous methods (Pandey & Kakar 1982; Smith 1998). It can also reduce the error caused by high frequency approximations. Split-Step Fourier Transform (SSFT) and finite difference algorithms is very popular for solving parabolic equation (Stogryn 1972). SSFT technique is frequency domain algorithm, when used to solve the PE, the step of SSFT is almost free from restrictions and can be selected as large discrete element. Therefore, the SSFT algorithm of PE is suitable for large scale wave propagation problems (Wilheit 1979; Williams 1971).

SSFT algorithm is complicated when dealing with irregular boundary, so it is not easy to be used in the calculation of electromagnetic scattering problems with complex structures (Militskii *et al.* 1978). Finite difference (FD) algorithm is carried out through the mesh of computation domain, and process computations according to the electromagnetic field on the adjacent grid-points. Since precise mesh is used, FD algorithm can directly calculate the field on arbitrary boundaries, therefore it is more convenient to deal with irregular boundaries, but the discretized step in FD is restricted by the wavelength (Militskii *et al.* 1978; Podzimek 1984).

Therefore, we must take small step, which results in large scale matrix operations. Solving the high-frequency, large-scale wave propagation problems based on PE, FD algorithm is slow and computer memory consumption is also high (Rose *et al.* 2002).

2. Split-step Padé Approximation

EM wave propagation on a foam-covered sea-surface is modelled by the standard parabolic wave equation (SPWE). The standard numerical simulation tool is the split-step Fourier method (SSFM), employing a fast Fourier transform (FFT) with complexity for discretization points at each propagation step. In this paper, an improved split-step method (SSM) employing Padé approximation to the exponential function reduces the simulation times by another 20%, without any degradation of the accuracy (Camps *et al.* 2005; Chen *et al.* 2003). In split-step Padé approach, higher order Padé approximations were magnitude faster than solutions based on Padé approximations that only considers asymptotic errors. The split-step Padé solution is valid for wide-angle propagation problems, waveguide properties with large depth variations and elastic ocean bottoms (Huang & Jin 1995; Tsang *et al.* 2000). Its solution has better efficiency compared to split-step Fourier method and practical global scale problems.

The split-step Padé method combines both the efficiency of the split-step Fourier method and the accuracy of the higher-order PEs. The algorithm is orders of magnitude faster than standard finite difference method and includes higher-order asymptotic (Guo *et al.* 2001). Furthermore, it allows for a powerful parallel implementation. Considering, a $3D$ SPE which satisfies the Helmholtz equation:

$$\psi_s = ik_0(-1+Q)\psi \tag{1}$$

where the pseudo-differential operator Q is defined by

$$Q = \sqrt{\frac{1}{k^2}\frac{\partial^2}{\partial x^2} + \frac{1}{k^2}\frac{\partial^2}{\partial y^2} + n^2} \tag{2}$$

The solution of equation (2) is given by

$$u(z+\Delta z, x, y) = \exp\big(ik\Delta z(Q-1)\big)\cdot u(z,x,y) \tag{3}$$

Equation (3) yields a more complex problem as the pseudo-differential square-root Q is associated with two transverse variables X and Y. For simplicity, X and Y were decoupled using the above equations.

$$X = \frac{1}{k^2}\frac{\partial^2}{\partial x^2} \tag{4}$$

$$Y = \frac{1}{k^2}\frac{\partial^2}{\partial y^2} + n^2 - 1 \tag{5}$$

Assuming the refractive index of the medium n is dependent on the depth z, that is X and Y commute. The exponential factors can be written as

$$e^{ik\Delta z(\sqrt{1+X+Y}-1)} \sim e^{ik\Delta z(\sqrt{1+X}-1)}e^{ik\Delta z(\sqrt{1+Y}-1)} \tag{6}$$

The equation (6) ignores coupling between X and Y. The approximation of X and Y by expanding the exponential factors using Taylor series yields.

$$u(z+\Delta z, x, y) = e^{\frac{ik\Delta z}{2}X}e^{\frac{ik\Delta z}{2}Y}\cdot u(z,x,y) \tag{7}$$

which takes the form of $3D$ narrow-angle PE

$$u_z = \frac{ik}{2}(X+Y)\cdot u \tag{8}$$

For wide-angle modelling, the square-root expressions in the X and Y are kept on the RHS of (6) or combining the narrow or wide-angle expressions (Lui et al. 2006; Wei & Liu 2007).

The split-step Padé algorithm helps to expand the exponential of the "propagator" which solves the Helmholtz equation (6). If the depth $z = m\Delta z$, where m is an integer, then the solution of (6) is expressed as

$$u(z+\Delta z, x) = \exp\Big(ik_0\Delta z\big(-1+\sqrt{1+X}\big)\Big)\cdot u(z,x) \tag{9}$$

The Padé approximation to the operator that propagates the solution in depth is applied on (9) to obtain

$$\exp\Big(ik_0\Delta z\big(-1+\sqrt{1+X}\big)\Big)\cdot u(z,x) \simeq 1 + \frac{\sum_{K=0}^{M} a_{k,M}\ X}{1+\sum_{K=1}^{N} b_{k,M}\ X} \tag{10}$$

$$\exp\Big(ik_0\Delta z\big(-1+\sqrt{1+X}\big)\Big)\cdot u(z,x) \simeq 1 + \prod_{K=0}^{M}\frac{1+\lambda_{K,M}X}{1+\mu_{K,M}X} \tag{11}$$

Substituting equation (10) into (9) we obtain the split-step Pade's solution

$$u(z+\Delta z, x) = u(z,x) + \frac{\sum_{K=0}^{M} a_{k,M}\ X}{1+\sum_{K=1}^{N} b_{k,M}\ X}\ u(z,x) \tag{12}$$

The $3D$ split-step Padé solution of (6) is obtained by expressing u in terms of the square-root operators X and Y.

$$u(z+\Delta z,x,y)=u(z,x,y)\left\{1+\frac{\sum_{K=0}^{M}a_{k,M}\ X}{1+\sum_{K=1}^{N}b_{k,M}\ X}\right\}$$
$$\cdot\,u(z,x,y)\left\{1+\frac{\sum_{K=0}^{M}a_{k,M}\ Y}{1+\sum_{K=1}^{N}b_{k,M}\ Y}\right\} \quad (13)$$

The product equation in $3D$ is written as

$$u(z+\Delta z,x,y)=u(z,x,y)\left\{1+\prod_{K=0}^{M}\frac{1+\lambda_{K,M}X}{1+\mu_{K,M}X}\right\}$$
$$\cdot\,u(z,x,y)\left\{1+\prod_{K=0}^{M}\frac{1+\lambda_{K,M}Y}{1+\mu_{K,M}Y}\right\} \quad (14)$$

and is not important for computation as the equivalent sum equation. This is because it does not allow parallel processing. Since $\mu_{K,M}$ and $\lambda_{K,M}$ are complex conjugates, we can say that the split-step Padé solution is stable (Wei & Ge 2005; Wei 2013).

2.1 The Depth Discretization of X and Y Operators

Equation (14) was numerically solved by discretizing the square-root operators X and Y in terms of the depth variables denoted by $X_{\Delta z}$ and $Y_{\Delta z}$ using finite difference schemes on $X_{\Delta z}$ and $Y_{\Delta z}$. Let's denote $\Delta z=\Delta x=h$ and represent $X_{\Delta x}=X_h$ and $Y_{\Delta x}=Y_h$. Discretization of the square-root variables X_h and Y_h using (4) and (5) yields.

$$X_h u_j^n=\frac{1}{k_0^2}D_h^2 u_j^n \quad (15)$$

$$Y_h u_j^n=\left(\frac{1}{k_0^2}D_h^2+n^2(z,x)-1\right)u_j^n \quad (16)$$

The standard second order central difference quotient was used to represent these discretized operators. The notation $u_j^n\sim u^n(z_j)$, $z_j=jh$, the central difference method of representing (15) and (16) are given below

$$X_h u_j^n=\frac{1}{k_0^2}\left(\frac{u_{j+1}^n-2u_j^n+u_{j-1}^n}{h^2}\right)=\frac{1}{k_0^2}\partial_z^2 u^n(z_j)+0(h^2) \quad (17)$$

$$Y_h u_j^n=\frac{1}{k_0^2}\left(\frac{u_{j+1}^n-2u_j^n+u_{j-1}^n}{h^2}\right)+\left(n^2(z,x)-1\right)u_j^n \quad (18)$$

The split-step Padé approach was used for the discretized depth operators X_h and Y_h, the propagated field along the positive direction can be obtained from Taylor series.

$$u^n(z_{j+1})=\exp(\pm h\partial_z)\,u^n(z_j)=\exp\left(\mp hk_0X^{\frac{1}{2}}\right)*\exp\left(\mp hk_0Y^{\frac{1}{2}}\right)u^n(z_j) \quad (19)$$

Using the equations

$$X_h = 2\frac{\cosh(\tau X^{1/2}-1)}{\tau_2} \tag{20}$$

$$Y_h = 2\frac{\cosh(\tau Y^{1/2}-1)}{\tau_2} \tag{21}$$

where $\tau = k_0 h$, and solving for X and Y by taking the inverse function of $cosh$ yields

$$X = \Gamma(X_h) = \tau^{-2} log^2\left\{1+\frac{\tau^2}{2}X_h + \sqrt{1+\frac{\tau^2}{2}X_h} - 1\right\} \tag{22}$$

$$Y = \Gamma(Y_h) = \tau^{-2} log^2\left\{1+\frac{\tau^2}{2}Y_h + \sqrt{1+\frac{\tau^2}{2}Y_h} - 1\right\} \tag{23}$$

substituting equations (22) and (23) into (6)

$$u_j^{n+1} = exp\left\{ik_0\Delta_z(-1+\sqrt{1+\Gamma(X_h)})\right\} * exp\left\{ik_0\Delta_z\left(-1+\sqrt{1+\Gamma(Y_h)}\right)\right\}u_j^n \tag{24}$$

Padé approximation is applied on (24) to obtain

$$exp\left\{ik_0\Delta_z(-1+\sqrt{1+\Gamma(X_h)})\right\} * exp\left\{ik_0\Delta_z\left(-1+\sqrt{1+\Gamma(Y_h)}\right)\right\}$$

$$\simeq \left\{1+\sum_{K=1}^{M}\frac{a_{K,M}X_h}{1+b_{K,M}X_h}\right\} * \left\{1+\sum_{K=1}^{M}\frac{a_{K,M}Y_h}{1+b_{K,M}Y_h}\right\} \tag{25}$$

Lastly, substituting equation (25) into (24)

$$u_j^{n+1} = \left\{1+\sum_{K=1}^{M}\frac{a_{K,M}X_h}{1+b_{K,M}X_h}\right\} * \left\{1+\sum_{K=1}^{M}\frac{a_{K,M}Y_h}{1+b_{K,M}Y_h}\right\}u_j^n \tag{26}$$

Padé coefficients are determined using

$$a_{K,M} = \left(\frac{2}{2M+1}\right)sin^2\left(\frac{k\pi}{2M+1}\right) \tag{27}$$

and

$$b_{K,M} = cos^2\left(\frac{k\pi}{2M+1}\right) \tag{28}$$

with M given as the number of terms in the Padé expansion. To evaluate the first 2M derivatives of Γ, Taylor series expansion is used and obtain a system of linear equations, that can be solved.

3. Evaluation of Effective Dielectric Constant of Sea-foam

Figures A-E comprise of 3D (three dimensions) slices of randomly packed spheres in a unit cube. These slices were later translated to 2D slices of randomly packed circles. The conversion of 3D randomly packed spheres to 2D packed circle was achieved by calculating the radii of each individual circle using the concept of intersection of a sphere and a plane. The 2D slices were discretized with grid sizes Δx and Δy which leads to intersection of the circles bounded in a unit square with some grid points. The grid sizes were sampled such that the edges of the circles circumference which intersects with grid points farther from the inner grids bounded by the circles are negligible.

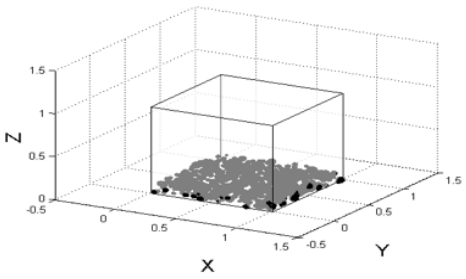

Figure A. Randomly packed spheres in slice 1

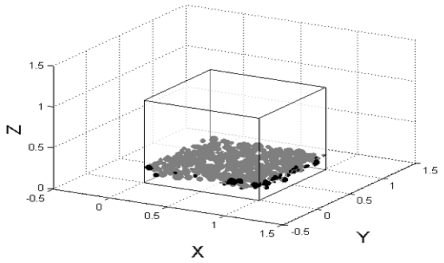

Figure B. Randomly packed spheres in slice 2

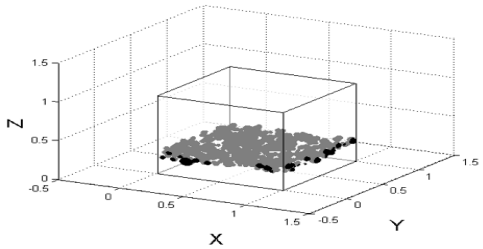

Figure C. Randomly packed spheres in slice 3

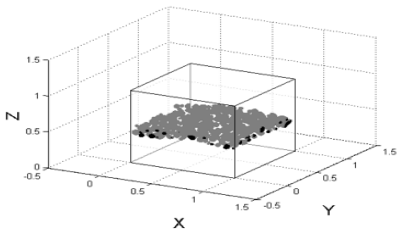

Figure D. Randomly packed spheres in slice 4

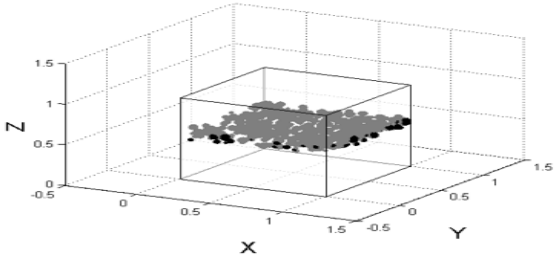

Figure E. Randomly packed spheres in slice 5

Estimate of the effective dielectric constant of sea foams were made by modelling the randomly packed bubbles as concentric circles in 2-D where the outer circle is a mixture of air and seawater while the inner circle contains about $(80-95)\ \%$ air. With these estimates we were able to calculate the area of the annulus (ring) as the radii of the outer circles are known.

The dielectric constant of seawater at fixed salinity $34\ psu$ and sea surface temperature $20°C$. The dielectric constant of air is taken as $1.00005 + 0.0000i$. The area of the circles in each slice was calculated using the total number of grid points.

The effective dielectric constants of sea foams at frequencies 10.7 GHz and 37.0 GHz were calculated for 5 slices of randomly packed air-bubbles coated with thin layer of seawater.

Table 1. Results for Dielectric constant of sea foam at frequencies of 10.7 GHz and 37 GHz for 5 2-D Slices of randomly packed air-bubbles covered with thin-layer of seawater.

FREQUENCY	10.7 GHz	37 GHz
Slice 1	1.0948-0.1251i	1.0006-0.0332i
Slice 2	1.1248-0.1507i	1.0108-0.0239i
Slice 3	1.1622-0.1810i	1.0225-0.0344i
Slice 4	1.1983-0.2072i	1.0315-0.0569i
Slice 5	1.2271-0.2277i	1.0465-0.0637i

4. Padé Approximation Computation for Investigation of Sea-foam Layer Model

The computer routines for propagation of EM wave through five (5) slices of sea-foam layer were written in Fortran 95 language with Silverfrost FTN95 compiler using a 64-bit machine in double precision. The Padé approximation method was used for observation of the amplitude and phase variations of the horizontal polarized (TE) and vertical polarized (TM) electric field due to its interaction with five (5) slices of sea-foam layer was coded in Matlab R2018b.

The Padé approximation routine was implemented to propagate the plane wave

$$E(z_0, x, y) = E(z, x, y)exp\left(ik_x x + ik_y y + ik_z z\right) \tag{29}$$

with $E(z, x, y) \approx 1$ along the forward $+z$ direction. The plane wave was propagated through the slices of sea foam layers each containing isotropically distributed air-bubbles. The slices are equally dimensioned with area $100\,mm \times 100\,mm$ with layer thickness $\delta_t = 10\,mm$ separating adjacent layers. The foam layer thickness $d \gg \lambda_0$ is required to account for attenuation and diffuse scattering as the incident E-field travels through slices of sea foam layer.

Investigation of the field perturbation at WindSat frequency channels of $10.7\,GHz$ and $37\,GHz$ were made by propagation of the E-field through slices of sea-foam layer. Given input parameters:

1. Speed of light $v = 2.99 \times 10^8\,ms^{-1}$
2. WindSat frequencies $f_1 = 10.7\,GHz$, and $f_2 = 37\,GHz$
3. Wavenumber $(\lambda_0 = v/f)$
4. $k - vector\ (k_0) = 2\pi/\lambda_0$
5. Refractive indices of the sea foam layer $n(z, x)$ in each slice of randomly distributed bubbles.
6. Dimension of scatterers $100\,mm \times 100\,mm \times 50\,m$
7. Foam layer thickness between adjacent slices (δ_t)

The incident wave was propagated at normal incidence and later tilted so that there is an initial phase gradient along the surface of the sea-foam model. This was achieved by assigning values of $0 \ll \theta_i \ll 90^\circ$ for the zenith angle and fixed azimuthal angle $\phi_i = 30^\circ$ or 45°.

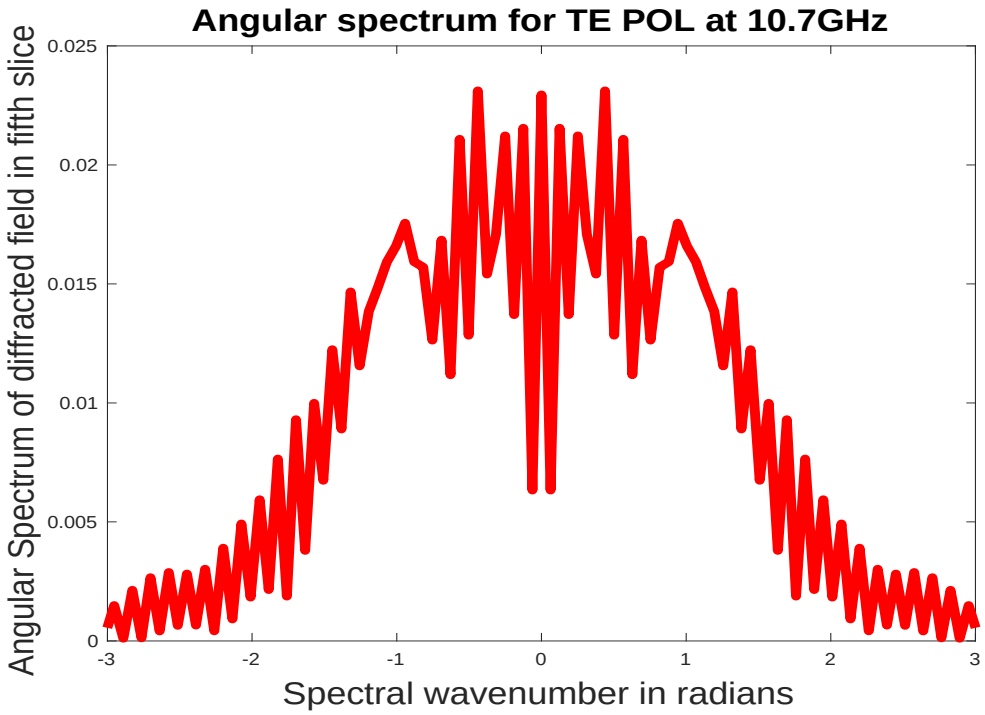

Figure 1. Plot of angular spectrum of diffracted field in fifth slice as a function of spectral wavenumber in radians for TE POL at 10.7 GHz

The amplitude of the E-field varies with angular wavenumber in radians as it propagates through slices of the sea foam layer. The figure above illustrates variation of angular spectrum of the E-field for TE polarization with spectral wavenumber in radians which describe diffuse scattering of the propagated E-field in different directions. We can see the fluctuation in peaks of the diffracted E-field is due to the random varying effective dielectric constants of sea-foam with varying size distributions.

Plane waves attenuate as they propagate through a lossy medium. From the expression of skin depth, it is found that the depth of penetration of fields in a lossy medium is inversely proportional to the square-root of the conductivity of the medium. In the extreme case of conductivity close to infinity, this depth vanishes and in fact, time varying fields and induced currents cannot exist within the medium. In other words, all fields and induced currents are confined near the skin region of the medium (Chen *et al.* 2000; Kong 2000).

It was observed that an increased high frequency resistance of a thin sea-foam layer, occurs as a result of current confinement through a smaller cross-section due to the skin effect.

In the ocean (seawater) with loss tangent greater than unity, we observe that attenuation of the E-field increased with depth. Antennas used for transmitting and receiving EM waves will cover more distance at lower propagating frequencies as the depth of penetration is inversely proportional to the attenuation constant. Attenuation is proportional to the square-root of the radian frequency in a lossy medium.

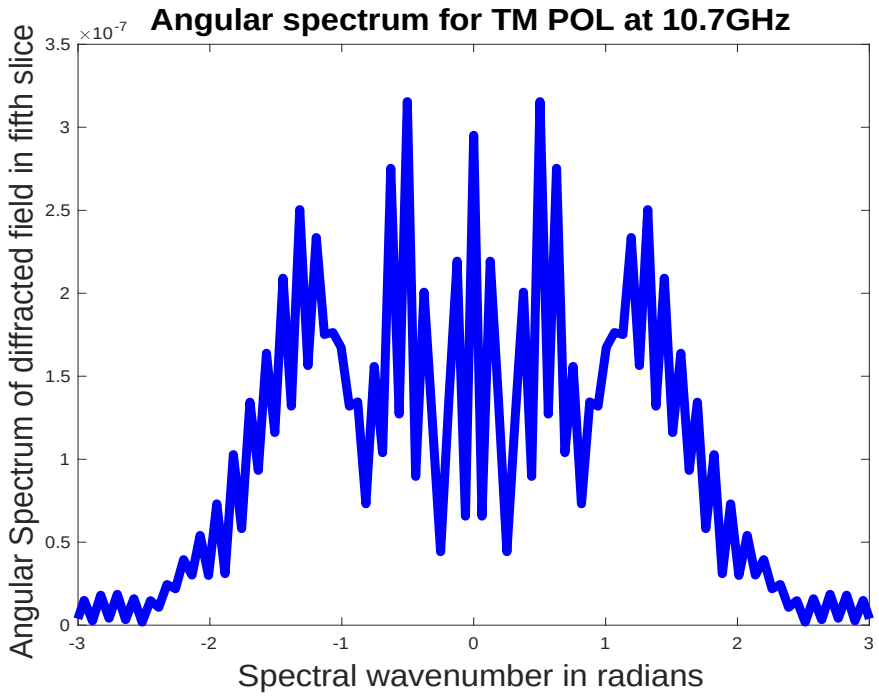

Figure 2. Plot of angular spectrum of diffracted field in fifth slice as a function of spectral wavenumber in radians for TM POL at 10.7 GHz

The angular spectrum of the diffused reflected wave field at $\delta_t = 2\,mm$ for deep phase scattering screen is a function of the spectral wavenumbers (p, q) for one dimensional $(1D)$ problem and (E_x, E_y) for two dimensional $(2D)$ problem in the X and Y directions. The broadening of the peaks in figures 2 and 3 depends on the diffraction factor $\exp(i\Delta z\sqrt{k^2 - (p^2 + q^2)})$. When k^2 approaches $(p^2 + q^2)$, the lobes of the angular spectrum are spread or broadened across the (p, q) or (E_x, E_y) spectral domain. This happens at low WindSat frequencies such as $6.8\,GHz$ and $10.7\,GHz$ but at higher frequencies such as $18.7\,GHz$, $23.8\,GHz$ and $37\,GHz$ where $k^2 \gg (p^2 + q^2)$, the lobes of the angular spectrum becomes sharper and narrower across the (p, q) or (E_x, E_y) spectral domain.

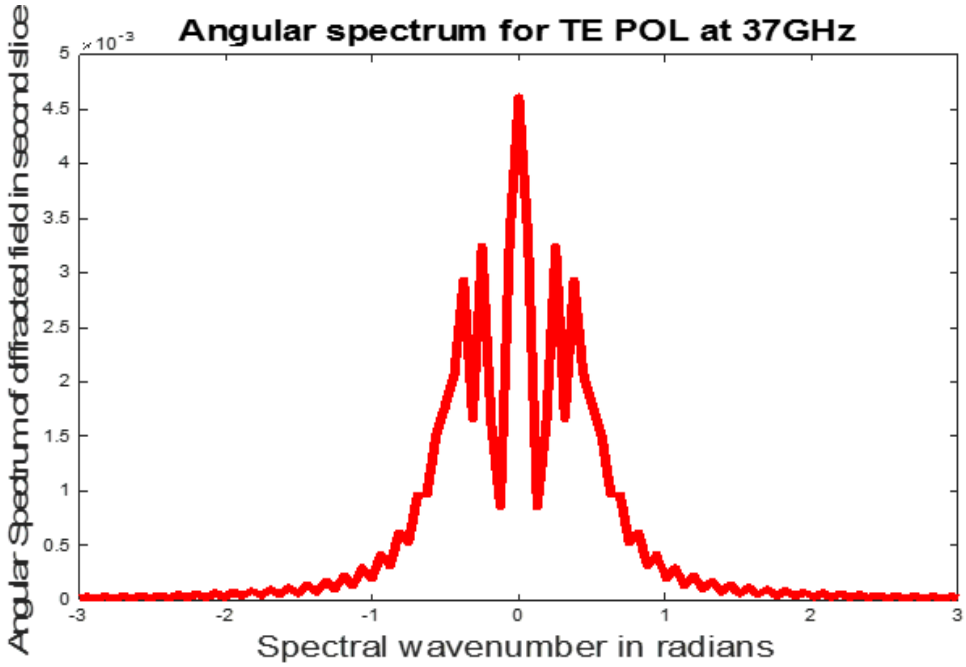

Figure 3. Plot of angular spectrum of diffracted field in second slice as a function of spectral wavenumber in radians for TE POL at 37 GHz

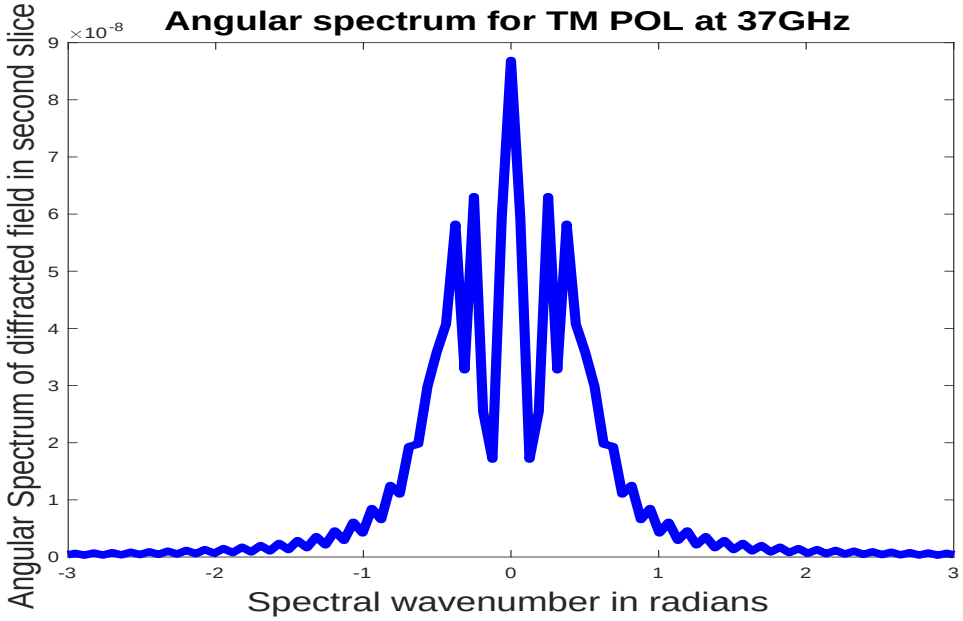

Figure 3. Plot of angular spectrum of diffracted field in second slice as a function of spectral wavenumber in radians for TM POL at 37 GHz

Figures 3 and 4 illustrate that the angular spectrum of diffracted field becomes narrower and sharper because the diffraction effects of the scattering due to plane wave propagation in a foam-covered sea-surface reduces with increase in frequency. This is due to the relationship between the wavenumber k and the spectral wavenumbers $(p^2 + q^2)$, where $k = 2\pi/\lambda$, implies that wavelength λ of the incident wave field decreases with increase in frequency. The wavenumber k increases with frequency. For deep phase scattering screen with thickness of foam layer $\delta_t = 2\ mm$, the dominant factor for attenuation of the wave field is absorption at the sea-surface.

5. Conclusion

Earlier reports suggest that there is negligible scattering due to interaction between EM wave and sea surface covered with foam and absorption been the major contributor to losses in a passive microwave remote sensing. This paper tends to show that with accurate prediction of the effective dielectric constant of sea foam based on its microscopic properties, we can investigate the scattering properties of the EM wave propagation in a foam-covered sea surface. In the future, we shall investigate the extinction properties of the sea foam layer by propagating an incident plane wave through the various 2-D slices using the Split-step Fourier method, and comparison of the SSFT results will be compared with Finite-difference method.

References

Camps, A., M. Vall-Llossera, R. Villarino, N. Reul, B. Chapron, I. Corbella, N. Duffo, F. Torres, J. J. Miranda, R. Sabia, et al., (2005): *The emissivity of foam-covered water surface at L-band: Theoretical modelling and experimental results from the frog 2003 field experiment*, Geoscience and Remote sensing, , **43**, no. 5, (925-937), *IEEE Transactions on*.

Chen, D., L. Tsang, L. Zhou, S. C. Reising, W. E. Asher, L. A. Rose, K.-H. Ding, and C.- T. Chen, (2003): *Microwave emission and scattering of foam based on Monte-Carlo simulations of dense media,* Geoscience and Remote sensing, **41**, no. 4, 782–790, *IEEE Transanction on*.

Chen, C.-T., et al., (2000): *Analytical and numerical methods for the scattering by* dense media, *Geoscience and Remote Sensing Symposium, Proceedings*, IGARSS, IEEE International, **5**.

Guo, J., L. Tsang, W. Asher, K.-H. Ding, and C.-T. Chen, (2001): *Applications of dense media radiative transfer theory for passive microwave remote sensing of foam-covered ocean," Geoscience and Remote Sensing, IEEE Transactions on*, **39**, no. 5, (1019–1027).

Huang, X. Z., and Y. Q. Jin, (1995): *Scattering and emission from two-scale randomly rough sea surface with foam scatterers Proc. Inst. Elect. Eng.*, **142**,109-114. *Microwave Antenna Propagat.*

Kong, J. A., 2000: Electromagnetic Wave Theory. Wiley-Inter-science, New York, 720.

Lui, S. B., Wei, E. B., Hong, J. L., & Ge, Y., (2006): *Microwave backscattering from the sea surface with breaking waves*, *Chinese Physics*, **15**, no. 9, (2175-2179).

Militskii, Y. A. et.al. (1978): *Atmospheric science: Thermal radio emission from foam structures, Sov. Phy.*: (23, 601-602), *Engl. Transl*.

Pandey, P.C., and R. K. Kakar, (1982). *Remote sensing of the ocean: An empirical microwave emissivity model for a foam-covered sea*. *7*, no.3, (135-140), *IEEE J. Oceanic Eng.*

Podzimek, J., (1984): *Geosci.: Size spectra of bubbles in the foam patches and sea salt nuclei over the surf zone,* (192-202), *Tellus* 36 *B*(3).

Rose, L. A., W. E. Asher, S. C. Reising, P. W. Gaiser, K. M. St Germain, D. J. Dowgiallo, K. A. Horgan, G. Farquharson, and E. Knapp, (2002): *Radiometric measurements of the microwave emissivity of foam, Geoscience and Remote Sensing,* no. 12, **40**, (2619-2625). *IEEE Transactions on***.**

Smith, P. M., (1998): *Remote sensing of the ocean:* The emissivity of sea foam at 19 and 37GHz, **26**, (541-547), *IEEE Trans. Geosci. Remote Sensing.*

Stogryn, A., (1972): *Remote sensing of the ocean:* The emissivity of sea foam at microwave frequencies, **77**, no. 9, (1658–1666). *Journal of Geophysical Research*.

Tsang, L., C-T. Chen, A. T. C. Chang, J. Guo, and K. H. Ding, (2000): *Dense media radiative transfer based on quasi-crystalline approximation with applications to passive microwave remote sensing of snow,* **35**, no. 3, 731-749, *Radio Sci.*

Wei, E. B., and Liu, Y., (2007): *Application of effective medium approximation theory to ocean remote sensing under wave breaking, Science in China Series D:* Earth Science, **50**, no. 3, (474-480).

Wei, E. B., and Ge, Y., (2005): *A microwave emissivity model of sea surface under wave breaking*, **34**, no. 6, (1259-1264), *Chinese Physics*.

Wei, E. B., (2013): *Effective medium approximation model of sea foam* layer *microwave emissivity of a vertical profile*, **34**, no. 4, (pp.1180-119) International Journal of Remote Sensing.

Wilheit Jr. T.T., (1979): *Ocean science: A model for the microwave emissivity of the ocean's surface as a function of wind speed*, *IEEE Trans.* **17,** (244-249), *Geosci. Electron*.

Williams, G.F.,(1971): *Remote sensing:Microwave emissivity measurements of bubbles and foam*. *Electron.,* **9**, (221-244) *IEEE Trans. Geosci.*.